

A new morphodynamic instability associated to the cross-shore transport in the nearshore

A. Falqués¹, F. Ribas¹, A. Mujal-Colilles² and C. Puig-Polo³

¹Physics Department, Universitat Politècnica de Catalunya, Campus Diagonal Nord, C. Jordi Girona, 1-3,
08034 Barcelona, Catalonia, Spain

²Department of Nautical Sciences and Engineering, Universitat Politècnica de Catalunya

³Department of Civil and Environmental Engineering, Universitat Politècnica de Catalunya

Key Points:

- The cross-shore sediment transport in the nearshore can be unstable in the along-shore direction
- The morphodynamic instability can develop only for beach profiles above the equilibrium profile
- This instability could explain transverse bar formation in shallow terraces at back-barrier beaches

Corresponding author: A. Falqués, albert.falques@upc.edu

Abstract

The existing theory for alongshore rhythmic bars relies on morphodynamic instabilities involving the wave-driven longshore current and rip currents. Transverse finger bars are common on coasts with a beach profile above the equilibrium profile (something not related to those currents). Here we show that under these conditions, the cross-shore transport can induce an instability which is triggered by the onshore transport together with wave refraction by the emerging bars. It is a finite amplitude instability, something not previously found in coastal geomorphology. We use a numerical model that filters out the dynamics associated to those currents. The alongshore spacing scales with the wavelength of the incident waves and the cross-shore extent is about the distance from shore to the depth of closure. The modelled bars compare qualitatively well with observations at El Trabucador back-barrier beach (Ebro delta, Western Mediterranean Sea).

Plain Language Summary

Beaches sometimes exhibit sand ridges (bars) nearly perpendicular to the shore that tend to be quite regularly spaced alongshore. Their spacing and cross-shore extent range from tens to thousands of meters. Intriguingly, these bars develop preferably at beaches with an abundant supply of sand such as delta barrier beaches, barrier islands and estuaries. Here we provide a possible explanation. Due to the sand excess, the bed in these beaches is very flat, the tendency for the sand to move downslope is very weak and the waves push the sand onshore. On the other hand, the waves refract, that is, their crest tip on deeper water propagates faster than the tip on shallower water. As a result, they turn towards the shallower areas and, thus, the onshore movement of the sand is deflected towards incipient shoals and accumulates there. This causes more intense wave refraction, which in turn brings more sand to the shallows, and so on. In this way, the bars can form out of small random irregularities in bed level.

1 Introduction

The beach morphology dynamics is the result of the interaction of water motion and sediment over a geological substratum. Coastal sediment transport is still poorly understood so that it largely relies on simplifications and parameterisations (Amoudry & Souza, 2011). At length scales comparable to the surf zone width or larger ($> 10\text{--}100$ m) the sediment transport can be conceptually decomposed into two main components. The *longshore transport* is driven by the surf-zone longshore current generated by breaking waves if they approach obliquely to the coast. The *cross-shore transport* is the main cause of the cross-shore beach profile sloping up onshore, sometimes with shore parallel sand bars. The main sources of cross-shore transport are the onshore transport driven by wave asymmetry and skewness, the offshore transport due to the undertow (bed-return current) and the downslope transport due to gravity (Fernández-Mora et al., 2015). An equilibrium bed profile is achieved if the three components are in balance. Finally, there are more contributions to sediment transport that do not fall into the longshore or cross-shore categories (e.g., those associated to the rip current circulation or to low frequency motions).

At sandy coasts, beach morphology is rarely uniform along the coast. Typically, the shoreline has undulations and the nearshore sea bed features shallows and deeps alongshore. Transverse bar systems (Ribas et al., 2015) are a well-known example encompassing a series of shallows or bars separated by deeps called rip channels (Figure 1). These systems are not only fascinating but also relevant from a practical point of view, essentially because they give information on morphodynamic processes of which they are the occasional visible imprint. The origin of coastal rhythmic patterns has been puzzling scientists for decades but there is nowadays the consensus that they emerge from feedbacks between hydrodynamics and morphology through the sediment transport (Coco & Mur-

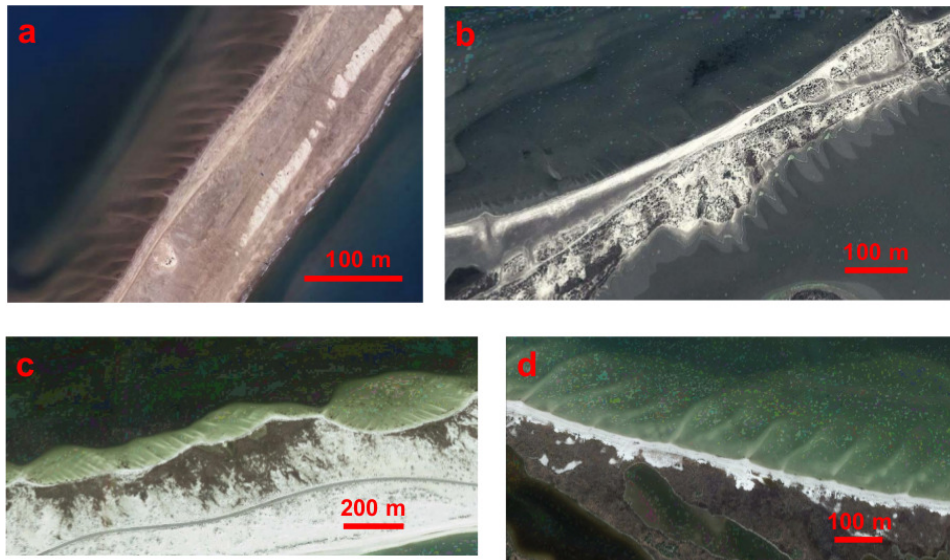


Figure 1. Shore-transverse finger sand bars in coasts with abundant sand supply. a) El Trabucador, Ebro delta, Catalonia, Spain ($40^{\circ} 36' 54''$ N , $0^{\circ} 43' 44''$ E). Source: Catalan Geographic and Geologic Institute, image from 2012. b) Beauduc Beach, Rhône Delta, France ($43^{\circ} 23' 41''$ N, $4^{\circ} 34' 35''$ E). Source: Google Earth, Maxar Technologies, image from 28/04/2010. Notice the bars (of different shape) at both sides of the barrier beach. c) Santa Rosa Island, Florida, USA ($30^{\circ} 22' 06''$ N, $86^{\circ} 57' 32''$ W). Source: Google Earth, Terrametrics, image from 15/01/2018. d) Horn Island, Mississippi, USA ($30^{\circ} 14' 38''$ N, $88^{\circ} 41' 06''$ W). Source: Google Earth, Landsat/Copernicus, image from 27/01/2015. The North in all plots is upward directed.

65 ray, 2007). Up to now, the self-organization mechanisms related with the sediment trans-
 66 port due to the longshore current and the rip currents have been largely explored while
 67 possible feedbacks arising from the cross-shore transport have been systematically ig-
 68 nored (Ribas et al., 2015). In fact, in the existing morphodynamic models the formation
 69 of rhythmic patterns occurs on top of a cross-shore profile that is assumed to be essen-
 70 tially in equilibrium. The net cross-shore transport is evaluated in a simplified way such
 71 that it only leads to a diffusive term in the equation governing bed evolution. Several
 72 studies with such models have been able to successfully describe the genesis of some types
 73 of transverse bars observed in nature (Ribas et al., 2015). However, the formation mech-
 74 anism for transverse finger bars in low-energy environments (Figure 1) remains mostly
 75 unexplained. In fact, observational studies on such transverse finger bars show that they
 76 develop preferably on gentle sloping beaches with abundant supply of sand (Niederoda
 77 & Tanner, 1970), probably with a beach profile above equilibrium (Evans, 1938). In this
 78 situation, the cross-shore transport dominates and thereby it might trigger a destabi-
 79 lizing mechanism instead of a damping one. Examples are the transverse finger bars along
 80 lake shores (Evans, 1938), estuaries (Eliot et al., 2006), barrier islands (Fig.1c,d) (Gelfenbaum
 81 & Brooks, 2003) and delta barrier beaches (Fig.1a,b) like El Trabucador back-barrier sys-
 82 tem, in the Ebro delta (Mujal-Colilles et al., 2019).

83 At its south west flank this delta has a long narrow spit, called El Trabucador, and
 84 its back-barrier beach is a shallow terrace of 100 m cross-shore up to 0.7 m depth, which
 85 face the semi-enclosed Alfacs bay. The sediment is fine sand and is provided by the open
 86 sea beach during overwash events. This beach is microtidal and wave energy is typically
 87 low due to the small fetch, with maximum heights ~ 0.6 m during NW wind and short

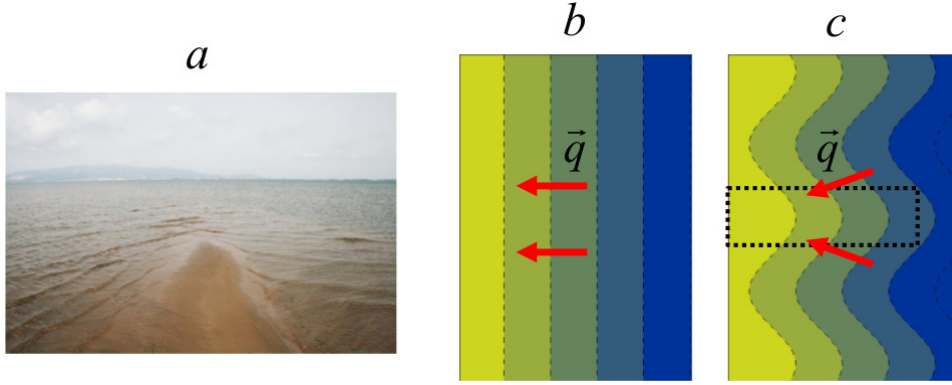


Figure 2. The morphodynamic instability mechanism: a) wave focusing by a shore-transverse sandbar due to topographic refraction in El Trabucador back-barrier beach, b) net onshore sediment transport for rectilinear shore-parallel depth contours above the equilibrium, and c) rotation of the cross-shore sediment flux for curvilinear depth contours and sediment convergence over the shoals (e.g., inside the dotted rectangle). In panels b) and c), yellow/blue colours mean shallow/deep water, respectively.

88 periods (< 3 s). Nevertheless, wave activity is intense enough to move the fine sand over
 89 all the terrace and a system of transverse finger bars is often present (Fig.1a). The along-
 90 shore wavelength is variable but the average and the most frequent is 20 m (Mujal-Colilles
 91 et al., 2019). The bars are thin and elongated with a cross-shore extent up to some 60 m
 92 and they commonly open an anti-clockwise angle of $10^\circ - 40^\circ$ with the shore normal.
 93 Field observations and aerial photos show that the system is persistent and dynamic. Typ-
 94 ically, waves refract in the proximity of the bars and wave crests cross each other over
 95 the bars thereby focusing their energy there (Fig.2a). This process, very noticeable and
 96 ubiquitous, was already described by Niederoda and Tanner (1970) as an important pro-
 97 cess for the formation and maintenance of transverse finger bars in other sites.

98 In this paper we present a new morphodynamic self-organization mechanism based
 99 on the cross-shore transport that could explain the generation of transverse finger bars
 100 in shallow terraces. The instability mechanism is described in section 2. Section 3 presents
 101 the model runs that confirm that, if the beach profile is above equilibrium, the cross-shore
 102 transport can generate shore-transverse sand bars similar to those observed at El Tra-
 103 bucador back-barrier beach. We use a morphodynamic model that has been validated
 104 with observations (Arriaga et al., 2017). The concluding remarks are given in section 4,
 105 along with the limitations and relevance of the model exercise.

106 2 The New Instability Mechanism

107 To describe the instability mechanism we consider an idealized rectilinear beach
 108 with an alongshore uniform bathymetry and waves incident normally to the shore. As-
 109 sume a cross-shore beach profile with a so gentle slope that it is above the equilibrium.
 110 Thereby, the gravity-driven transport is small and the net depth-averaged cross-shore
 111 sediment flux, \bar{q} , is onshore directed, dominated by wave asymmetry and skewness (Fig-
 112 ure 2b). Assume now a shoal breaking the alongshore uniformity. The waves propaga-
 113 ting in the vicinity of the shoal will refract so that the wave crests at both sides of the
 114 shoal will veer towards the shallower part (Figure 2a). As a result, the cross-shore sed-
 115 iment flux will veer towards the shallower region too bringing sediment to it. This will
 116 swell the shoal so that a positive feedback will occur (Figure 2c). If the cross-shore pro-

117 file is so steep that it is below the equilibrium, the net cross-shore transport is dominated
 118 by gravity (hence seaward directed) and the situation is just opposed.

119 The instability mechanism can be mathematically described with an idealized mor-
 120 phodynamic equation associated to the cross-shore transport. This also facilitates un-
 121 derstanding the essential differences with the usual approach where the cross-shore trans-
 122 port plays a diffusive role. We consider a Cartesian coordinate system (x, y, z) , x point-
 123 ing seawards, y along the shoreline and z upwards, $z=0$ being the mean sea level. We
 124 represent the cross-shore sediment transport as

$$125 \quad \vec{q} = q_w \frac{\vec{k}}{k} - \gamma \nabla z_b \quad (1)$$

126 where q_w is the onshore wave-driven transport module, \vec{k} is the wavenumber vector, $\gamma >$
 127 0 is a wave stirring factor and $z = z_b(x, y, t)$ is the bed level. These are the only two terms
 128 (the wave-driven and the gravitational) needed to capture the essence of the new insta-
 129 bility. Other contributions to cross-shore transport, like undertow or infragravity waves,
 130 or the sediment transport by the currents are ignored in this section. We consider the
 131 shoreline, $y=0$, and an alongshore uniform bathymetry, $z_b = Z(x)$, as a reference beach
 132 state, not necessarily in equilibrium. The local reference beach slope is $\beta(x) = -dZ(x)/dx$.
 133 In the reference state we assume shore-normal incident monochromatic waves.

134 Let us consider now a small alongshore irregularity of the reference state, $h(x, y, t)$,
 135 so that $z_b(x, y, t) = Z(x) + h(x, y, t)$. It is important to realize that although h is as-
 136 sumed to be infinitesimal, the perturbation with respect to the equilibrium, $Z(x) - Z_e(x) +$
 137 $h(x, y, t)$ is not. Let θ and ϕ be the (small) angles between ∇z_b and \vec{k} and the $-x$ axis,
 138 respectively, that is,

$$139 \quad \nabla z_b = |\nabla z_b|(-\cos \theta \hat{e}_x + \sin \theta \hat{e}_y) \quad , \quad \vec{k} = k(-\cos \phi \hat{e}_x + \sin \phi \hat{e}_y) \quad (2)$$

140 where \hat{e}_x, \hat{e}_y are the unit vectors along the x, y axes. Introducing this in the sediment
 141 transport one obtains

$$142 \quad \vec{q} = q_w^0(-\cos \phi \hat{e}_x + \sin \phi \hat{e}_y) + \gamma^0 \beta \hat{e}_x - \gamma^0 \nabla h \quad (3)$$

143 where q_w^0 and γ^0 are the magnitudes of the wave-driven transport and the stirring in the
 144 reference state. The perturbations in q_w and γ have been here neglected for simplicity,
 145 as done in most morphodynamic models (Ribas et al., 2015). Then, by keeping only zero
 146 and first order terms,

$$147 \quad \vec{q} = Q \hat{e}_x + q_w^0 \phi \hat{e}_y - \gamma^0 \nabla h \quad (4)$$

148 with $Q = \gamma^0 \beta - q_w^0$ being the net transport in the reference state. Due to topographic
 149 refraction, the wave fronts tend to become parallel to the depth contours. We can there-
 150 fore assume $\phi = \mu \theta$ with $0 < \mu(x, y) < 1$. In fact, $\phi(x, y)$ is not a local function of
 151 $\theta(x, y)$, since it depends on the whole wave refraction from offshore to the (x, y) loca-
 152 tion, but for our purpose and for small angles this assumption seems reasonable. Fur-
 153 thermore, to first order, equation (2) leads to

$$154 \quad \theta = \frac{1}{\beta} \frac{\partial h}{\partial y} \quad (5)$$

155 Finally, by invoking the sediment conservation equation:

$$156 \quad \frac{\partial z_b}{\partial t} + \frac{1}{1-p} \nabla \cdot \vec{q} = 0 \quad (6)$$

157 with p being the bed porosity, one obtains the following morphodynamic governing equa-
 158 tion:

$$159 \quad (1-p) \frac{\partial h}{\partial t} = \frac{\partial}{\partial x} \left(\gamma^0 \frac{\partial h}{\partial x} \right) + \frac{\partial}{\partial y} \left(\gamma^0 (1-\alpha) \frac{\partial h}{\partial y} \right) - \frac{dQ}{dx} \quad (7)$$

160 where $\alpha = \mu q_w^0 / (\gamma^0 \beta)$. This is a diffusion equation where the cross-shore and the along-
 161 shore diffusivities are γ^0 and $\gamma^0(1 - \alpha)$, respectively. If the reference state is an equi-
 162 librium one, $Q = 0$, and wave refraction is neglected, $\mu = 0$, both diffusivities in the
 163 governing equation (7) are equal and positive. This is the standard approach in which
 164 any bathymetric perturbation tends to damp (Ribas et al., 2015). Including wave refrac-
 165 tion reduces the alongshore diffusivity but, if the reference state is an equilibrium one,
 166 the alongshore diffusivity is still positive. However, if the reference profile is above equi-
 167 librium, the net cross-shore transport is positive, $q_w^0 > \gamma^0 \beta$ and the the alongshore dif-
 168 fusivity may become negative. In this case, alongshore irregularities can grow by insta-
 169 bility.

170 3 Morphodynamic Model Runs

171 3.1 Brief Model Description

172 To study in more detail how the instability mechanism works and is able of gener-
 173 ating alongshore rhythmic morphology we use the so-called Q2Dmorfo model (Arriaga
 174 et al., 2017). This model computes the evolving bathymetry in a rectangular domain un-
 175 der certain wave forcing. The main inputs are the initial bathymetry, the wave forcing
 176 and an assumed equilibrium beach profile. From this, the model computes the wave field
 177 inside the domain and the sediment flux, and it updates the bathymetry at each time
 178 step from the sediment conservation equation (6). The model is similar to other exist-
 179 ing 2DH morphodynamic models except that it computes the sediment flux directly from
 180 the wave field in a parametric way without resolving the surf zone hydrodynamics. By
 181 paying the price of missing some important surf zone processes (like rip currents) it is
 182 able to describe the large scale coastal evolution at time scales of decades-centuries. Al-
 183 though we are here interested in length scales much smaller than those for which the model
 184 is designed, we use it for two reasons. First, it describes the cross-shore transport as pro-
 185 portional to the deviation of the local beach slope with respect to the equilibrium one.
 186 Second, it filters out the rip current circulation which is another known factor of along-
 187 shore rhythmic morphology. Therefore, the mechanism associated to the cross-shore trans-
 188 port can be analyzed in isolation.

189 The model is here briefly described, mainly indicating how the sediment fluxes are
 190 calculated from the wave field. More details can be found in Arriaga et al. (2017). We
 191 use the same coordinate system introduced in section 2 and a computational domain $0 \leq$
 192 $x \leq L_x, 0 \leq y \leq L_y$, including emerged and submerged beach. The depth-integrated
 193 sediment flux is decomposed into three components,

$$194 \quad \vec{q} = \vec{q}_L + \vec{q}_C + \vec{q}_D \quad (8)$$

195 The first one is a parameterization of the longshore sediment flux driven by the break-
 196 ing waves. The second one is the cross-shore transport and reproduces the tendency of
 197 the beach to evolve towards the equilibrium profile. The third term is an alongshore dif-
 198 fusive transport to account for the hydrodynamic smoothing of small scale bathymet-
 199 ric noise. The cross-shore and alongshore directions for an undulating coast loose the clear
 200 meaning they have for a rectilinear coast. However their meaning can be recovered from
 201 the mean trend of the bathymetric contours if the small scale bathymetric features are
 202 filtered out. Also, these averaged contours are those felt by wave propagation and trans-
 203 formation. Therefore, from the actual bathymetry, $z_b(x, y, t)$, an averaged bathymetry,
 204 $\bar{z}_b(x, y, t)$, is defined by using a running average in a rectangular window of size a_x and
 205 a_y , which are at least of the order of the wavelength. Then, we define the local mean "cross-
 206 shore" direction by the unit vector

$$207 \quad \hat{n} = -\frac{1}{|\nabla \bar{z}_b|} \nabla \bar{z}_b \quad (9)$$

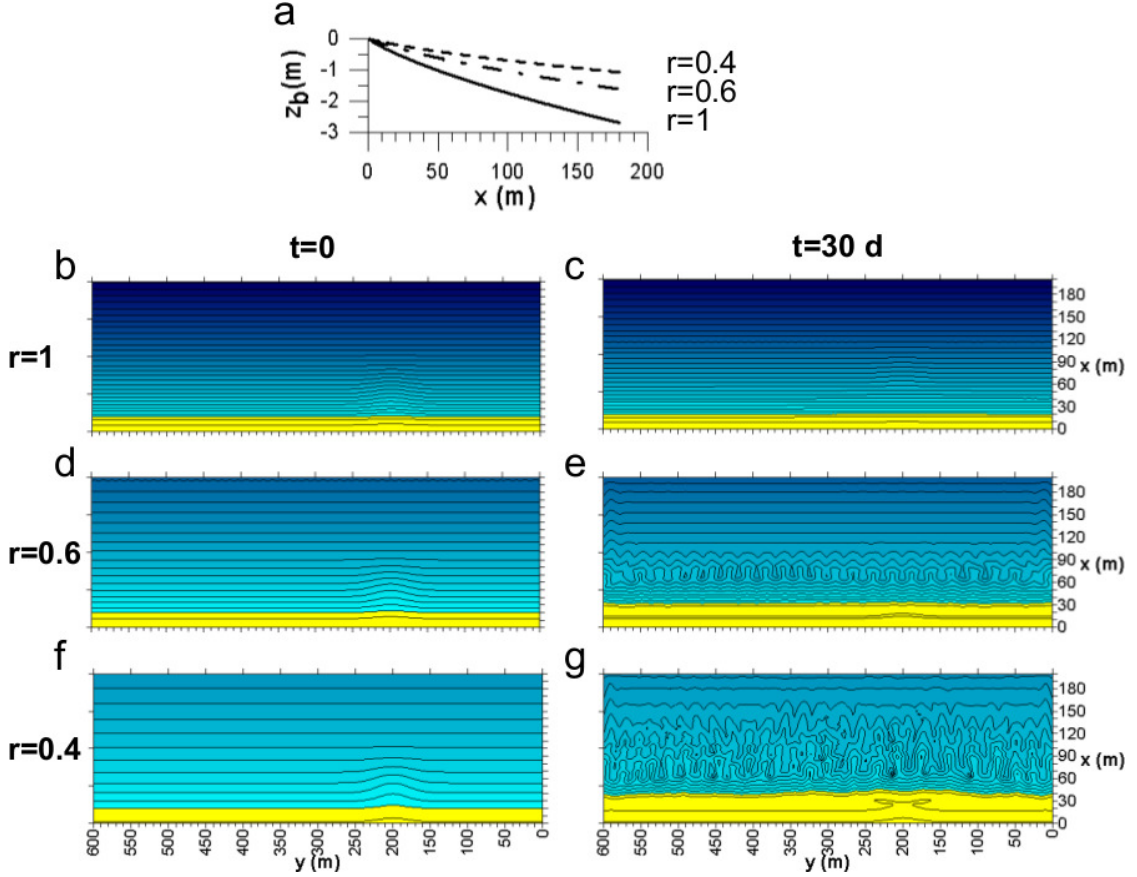


Figure 3. Sensitivity to the initial beach slope: a) Initial profile for $r = 1$ in solid line (which is also the equilibrium profile), and for $r = 0.6$ and $r = 0.4$, and b)-g) Q2Dmorfo result for the three r values. Panels b), d) and f) are the initial bathymetry and panels c), e) and g) are the bathymetries at $t = 30$ d. Yellow and blue colours represent the emerged and submerged beach, respectively, and depth contours are plotted every 0.1 m.

208 The cross-shore transport in equation (8) is proportional to the difference between
 209 the local equilibrium slope, $\beta_e(D)$, and the actual slope in the local cross-shore direc-
 210 tion,

$$211 \quad \vec{q}_C = -\gamma_C(\hat{n} \cdot \nabla z_b + \beta_e) \hat{n} \quad (10)$$

212 The water depth is $D = -z_b$ and $\gamma_C(D)$ is a wave stirring factor. The depth where γ_C
 213 magnitude is 0.02 times its shoreline value is the depth of closure, D_c . Note that equa-
 214 tion (10) implies that the wave-driven transport is up-slope the averaged bathymetry which,
 215 in the framework of section 2, is equivalent to the limit case $\mu = 1$, that is, $\phi = \theta$.

216 Model runs are done keeping in mind the geometry and typical wave conditions at
 217 El Trabucador back-barrier beach. A rectangular domain $L_x = 200$ m (cross-shore), $L_y =$
 218 600 m (longshore), with a dry beach width of 20 m. As equilibrium profile, we consider
 219 a shifted Dean profile (Falqués & Calvete, 2005)

$$220 \quad Z_e(x) = -B \left((x + x_0)^{2/3} - x_0^{2/3} \right) \quad (11)$$

221 The parameters, $B = 0.095 \text{ m}^{1/3}$ and $x_0 = 9.42$ m, are chosen to obtain a shoreline slope
 222 $\beta_s = 0.03$ and to approximate a Dean profile far from the shoreline, $Z_d = -Ax^{2/3}$, with

223 $A = 0.084 \text{ m}^{1/3}$ (value coherent with a sediment grain size of $d_{50} \approx 0.15 \text{ mm}$ (Dean &
 224 Dalrymple, 2002)). The imposed values for β_s and d_{50} are obtained from El Trabucador
 225 data (Mujal-Colilles et al., 2019). The initial bathymetry for the model runs is

$$226 \quad z_b(x, y, 0) = rZ_e(x) + h(x, y) \quad (12)$$

227 where $h(x, y)$ is a small localized perturbation and r controls whether the initial profile
 228 is above ($r < 1$) or below ($r > 1$) equilibrium (Figure 3a,b). A value $r \approx 0.4$ is obtained
 229 when the shifted Dean profile to the observed profile at El Trabucador, and it is used
 230 as default value. It also indicates that the observed profile is clearly above the equilib-
 231 rium profile that would correspond to its grain size. As default wave forcing we use con-
 232 stant wave conditions characteristic from El Trabucador, $H_s = 0.28 \text{ m}$, $T_p = 2 \text{ s}$ (Mujal-
 233 Colilles et al., 2019), and shore-normal incidence, $\theta = 0$. The default bathymetric smooth-
 234 ing box is $a_x = 3 \text{ m}$ and $a_y = 10 \text{ m}$, and the closure depth is estimated out of the data,
 235 $D_c = 0.8 \text{ m}$. The spatial grid is defined by $dx = 0.5 \text{ m}$ and $dy = 1.5 \text{ m}$ and the time
 236 step is $dt = 0.00002 \text{ d}$.

237 3.2 Model Results

238 For $r = 1$ the initial perturbation tends to smooth out and the bathymetric con-
 239 tours become rectilinear and parallel to the shoreline (Figure 3b,c). The initial morphol-
 240 ogy is clearly stable. In contrast, for $r = 0.4$ undulations develop in the depth contours
 241 (Figure 3f,g). Quite rapidly, the amplitude of the undulations increases and a complex
 242 bathymetry encompassing shore-transverse bars appears in the shoaling zone. Thus, the
 243 initial morphology is clearly unstable. At some spots, the morphology is relatively regu-
 244 lar but at others it is quite complex with several length scales. However, an alongshore
 245 length scale $L \approx 25 \text{ m}$ becomes apparent. Also, the shoreline progrades, which is con-
 246 sistent with the beach being under accretive conditions. A detailed description of the
 247 time evolution of the morphology in the default case can be found in the Supporting In-
 248 formation. For $r = 0.5-0.7$ something similar occurs but at a slower rate as r increases.
 249 For $r = 0.7$ only some weak undulations in the depth contours have developed after 30
 250 days. In contrast, the behaviour for $r = 0.8$ is similar to $r = 1$. Thus, it is found that
 251 the instability develops if the profile is above equilibrium but with a certain threshold.

252 To discard that the instability is a numerical artifact, the sensitivity to the numer-
 253 ical parameters is investigated. Little sensitivity is found by taking $dy = 0.5 - 1.5 \text{ m}$
 254 or changing the size of the domain, $L_y = 300 - 600 \text{ m}$. Also results do not depend on
 255 the initial perturbation (three cases have been analysed, see the Supporting Information
 256 for details). The particular morphology is somewhat different, but the qualitative be-
 257 haviour is the same. The sensitivity to the averaging box size, a_x, a_y , has been carefully
 258 examined. It is found that a_x hardly influences the results but a_y has a strong influence
 259 on the shape and wavelength of the transverse bar system. For small a_y the morphol-
 260 ogy is quite complex and noisy, and the spacing between the bars is small. In contrast,
 261 as a_y increases, it becomes smoother and the spacing increases (see Figure 4a,b). Indeed,
 262 it is found that wavelength increases (roughly) linearly with a_y (see the Supporting In-
 263 formation for details). For $a_y > 50 \text{ m}$, bars do not grow inside the domain. The depen-
 264 dence of the results on a_y is discussed in Section 4.

265 Regarding the wave conditions, the values $H_s = 0.14 - 0.42 \text{ m}$ and $T_p = 1 - 3 \text{ s}$
 266 are tested and results hardly change (more details in the Supporting Information). More
 267 influence have D_c and θ . The values $D_c = 0.6-1.2 \text{ m}$ have been examined and its pri-
 268 mary influence is an increase of the cross-shore length of the bars with increasing D_c (Fig-
 269 ure 4c,d). It is seen that for oblique wave incidence, bars grow faster and tend to be aligned
 270 against the wave incidence (Figure 4e,f). Morphodynamic noise appears much sooner
 271 than for shore normal wave incidence and the model breaks down earlier (for example
 272 at $t = 15 \text{ d}$ for $\theta = 10^\circ$ but as soon as $t = 2 \text{ d}$ for $\theta = 40^\circ$).

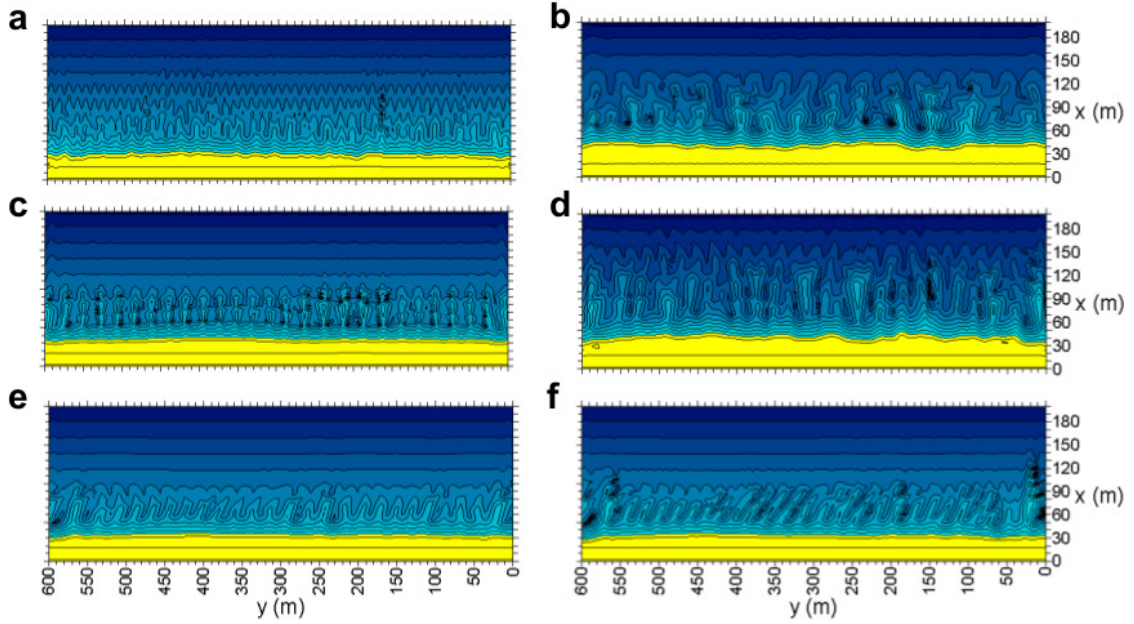


Figure 4. Q2Dmorfo result for (a) $a_y = 5$ m and (b) $a_y = 20$ m, both at $t = 20$ d, for (c) $D_c = 0.6$ m and (d) $D_c = 1$ m, both at $t = 19$ d, and for (e) $\theta = 10^\circ$ and (f) $\theta = 20^\circ$, both at $t = 2$ d. The other parameters have their default values. Yellow and blue colours represent the emerged and submerged beach, respectively, and depth contours are plotted every 0.1 m. In case of non shore-normal wave incidence, waves came from the right on the plot.

273

4 Final Remarks

274

275

276

277

278

279

280

The resulting onshore sediment transport on beaches that are significantly shallower than the equilibrium bathymetric profile can produce an instability that breaks the alongshore uniformity. This mechanism can explain the quite common existence of transverse finger bars in shallow areas with an abundant supply of sand in delta barrier beaches, barrier islands and estuaries. The instability occurs because wave refraction rotates the wave fronts towards the growing transverse bars so that the onshore transport veers too and causes flux convergence over the bars.

281

282

283

284

285

286

287

288

289

290

291

292

293

294

It is remarkable that, despite the present modelling approach is just meant to capture the essence of the instability in a qualitative way, the modelled morphology bears a reasonable similitude with the transverse bars shown in Figure 1. Moreover, the model application to El Trabucador gives emerging length scales which are consistent with those observed in this site. The dominant alongshore spacing between the bars, L , increases linearly with the alongshore length of the smoothing box, a_y . The latter must be of the order of the minimum alongshore length scale of the bathymetric features that can affect wave refraction, which is difficult to ascertain but must be of the order of the wavelength of the wave forcing. At the water depths $D \approx 0.4 - 0.6$ m where the bars form, waves with $T_p = 2 - 3$ s have wavelengths in the range 4 - 7 m which would be an appropriate range for a_y too. Alongshore wavelengths $L \approx 16 - 19$ m are then obtained, which are consistent with the most frequent bar spacing at El Trabucador. Regarding the cross-shore extent of the bars, it is controlled by the depth of closure, D_c , and a value of about 60 - 90 m is found for this site (the maximum observed one is about 60 m).

295

296

Although we have focused here on illustrating the capability of the present mechanism to generate transverse finger bars in areas of sand excess it could also influence

297 the down-state sequence under accretive conditions in any beach (Wright & Short, 1984)
 298 and the development of, e.g., crescentic bars (Dubarbier et al., 2017). This should be in-
 299 vestigated with a surf (and shoaling) zone morphodynamic model incorporating a pa-
 300 rameterization of cross-shore transport capable of accounting for the present instabil-
 301 ity mechanism in open ocean beach environments.

302 The instability concept had been applied to explain the formation of beach cusps
 303 (Dodd et al., 2008), crescentic bars (Garnier et al., 2008), shore-transverse bars (Ribas
 304 et al., 2012), shoreline sand waves and large scale cusped features (and spits) (Ashton
 305 et al., 2001). In all these cases the morphological features develop out of an equilibrium
 306 state, i.e., time invariant, both in the case of linear or nonlinear analysis. In contrast,
 307 the new instability develops from a morphology which is necessarily not an equilibrium
 308 state. In this sense, it is a finite-amplitude instability, i.e., it can not be captured by the
 309 usual linear stability analysis of an equilibrium morphology. Finite-amplitude instabil-
 310 ities are common in other fields of Physics (Drazin & Reid, 1981; Grossmann, 2000; Eck-
 311 hardt et al., 2007) but, to our knowledge, they had not been found so far in coastal ge-
 312 omorphology.

313 Acknowledgments

314 Datasets from El Trabucador back-barrier beach are included in this paper: Mujal-Colilles
 315 et al. (2019) This research is part of the Spanish Government projects CTM2015-66225-
 316 C2-1-P and RTI2018-093941-B-C33 (MINECO/FEDER). .

317 References

- 318 Amoudry, L. O., & Souza, A. J. (2011). Deterministic coastal morphological and
 319 sediment transport modeling: A review and discussion. *Reviews of Geophysics*,
 320 *49*(2). doi: 10.1029/2010RG000341
- 321 Arriaga, J., Rutten, J., Ribas, F., Ruessink, B., & Falqués, A. (2017). Modeling the
 322 longterm diffusion and feeding capability of a mega-nourishment. *Coast. Eng.*,
 323 *121*, 1-13.
- 324 Ashton, A., Murray, A. B., & Arnault, O. (2001). Formation of coastline features by
 325 large-scale instabilities induced by high-angle waves. *Nature*, *414*, 296-300.
- 326 Coco, G., & Murray, A. B. (2007). Patterns in the sand: From forcing templates to
 327 self-organization. *Geomorphology*, *91*(271-290).
- 328 Dean, R. G., & Dalrymple, R. A. (2002). *Coastal processes*. Cambridge: Cambridge
 329 University Press.
- 330 Dodd, N., Stoker, A., Calvete, D., & Sriariyawat, A. (2008). On beach cusp forma-
 331 tion. *J. Fluid Mech.*, *597*, 145-169.
- 332 Drazin, P. G., & Reid, W. H. (1981). *Hydrodynamic Stability*. Australia: Cambridge
 333 University Press.
- 334 Dubarbier, B., Castelle, B., Ruessink, G., & Mariou, V. (2017). Mechanisms control-
 335 ling the complete accretionary beach state sequence. *Geophys. Res. Lett.*, *44*.
 336 (doi:10.1002/2017GL073094)
- 337 Eckhardt, B., Schneider, T. M., Hof, B., & Westerweel, J. (2007). Turbulence transi-
 338 tion in pipe flow. *Ann. Rev. Fluid Mechanics*, *39*, 447-468.
- 339 Eliot, M. J., Travers, A., & Eliot, I. (2006). Morphology of a Low-Energy Beach,
 340 Como Beach, Western Australia. *J. Coastal Res.*, *22*(1), 63-77.
- 341 Evans, O. F. (1938). The classification and origin of beach cusps. *J. Geology*, *46*,
 342 615-627.
- 343 Falqués, A., & Calvete, D. (2005). Large scale dynamics of sandy coast-
 344 lines. Diffusivity and instability. *J. Geophys. Res.*, *110*(C03007).
 345 (doi:10.1029/2004JC002587)
- 346 Fernández-Mora, A., Calvete, D., Falqués, A., & de Swart, H. E. (2015). Onshore
 347 sandbar migration in the surf zone: New insights into the wave-induced sedi-

- 348 ment transport mechanisms. *Geophysical Research Letters*, *42*(8), 2869-2877.
349 doi: 10.1002/2014GL063004
- 350 Garnier, R., Calvete, D., Falqués, A., & Dodd, N. (2008). Modelling the formation
351 and the long-term behavior of rip channel systems from the deformation of a
352 longshore bar. *J. Geophys. Res.*, *113*(C07053). (doi:10.1029/2007JC004632)
- 353 Gelfenbaum, G., & Brooks, G. R. (2003). The morphology and migration of trans-
354 verse bars off the west-central florida coast. *Mar. Geol.*, *200*, 273-289.
- 355 Grossmann, S. (2000). The onset of shear flow turbulence. *Reviews of Modern*
356 *Physics*, *72*(2), 603-618.
- 357 Mujal-Colilles, A., Grifoll, M., & Falqués, A. (2019). Rhythmic morphology in a mi-
358 crotidal low-energy beach. *Geomorphology*, *334*, 151-164. doi: doi.org/10.1016/
359 j.geomorph.2019.02.037
- 360 Niederoda, A. W., & Tanner, W. F. (1970). Preliminary study on transverse bars.
361 *Mar. Geol.*, *9*, 41-62.
- 362 Ribas, F., de Swart, H. E., Calvete, D., & Falqués, A. (2012). Modeling and an-
363 alyzing observed transverse sand bars in the surf zone. *J. Geophys. Res.*,
364 *117*(F02013). (doi:10.1029/2011JF002158)
- 365 Ribas, F., Falqués, A., de Swart, H. E., Dodd, N., Garnier, R., & Calvete, D. (2015).
366 Understanding coastal morphodynamic patterns from depth-averaged sediment
367 concentration. *Rev. Geophys.*, *53*. (doi:10.1002/2014RG000457)
- 368 Wright, L. D., & Short, A. D. (1984). Morphodynamic variability of surf zones and
369 beaches: A synthesis. *Mar. Geol.*, *56*, 93-118.

Figure 1.

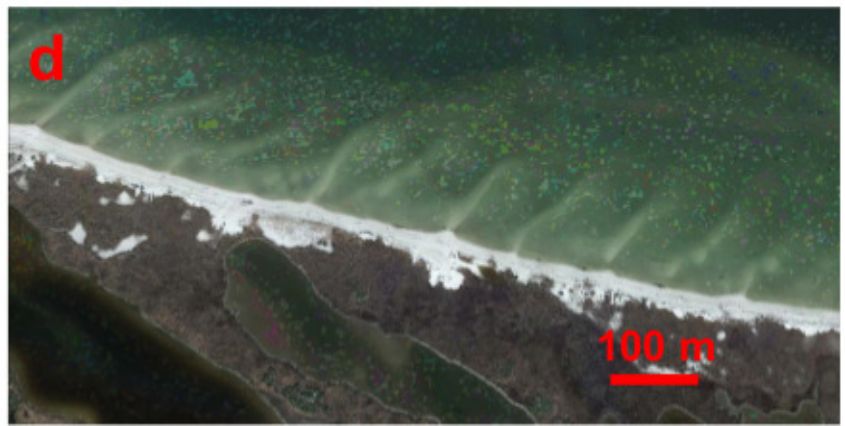
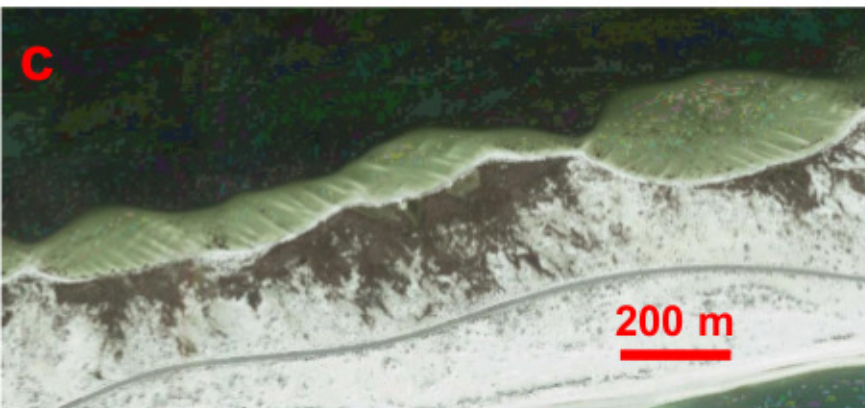
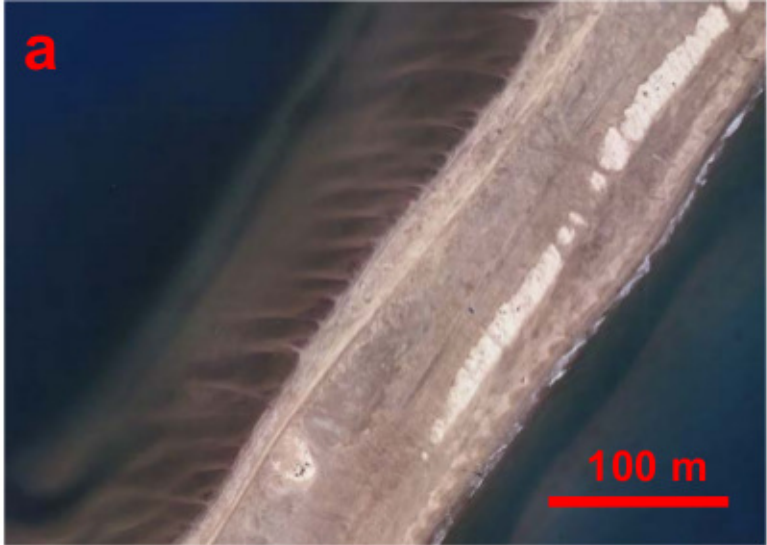
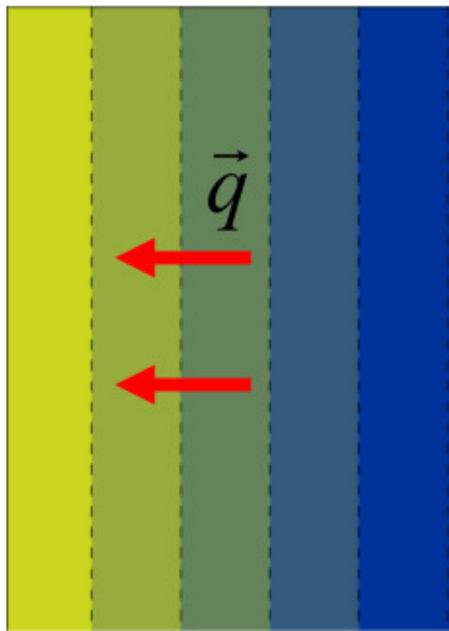


Figure 2.

a



b



c

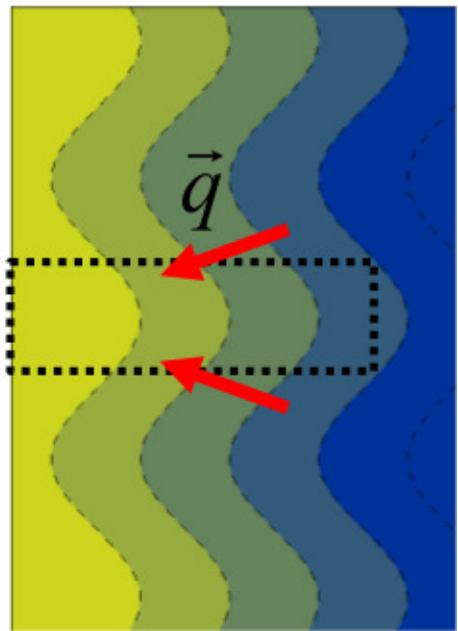


Figure 3.

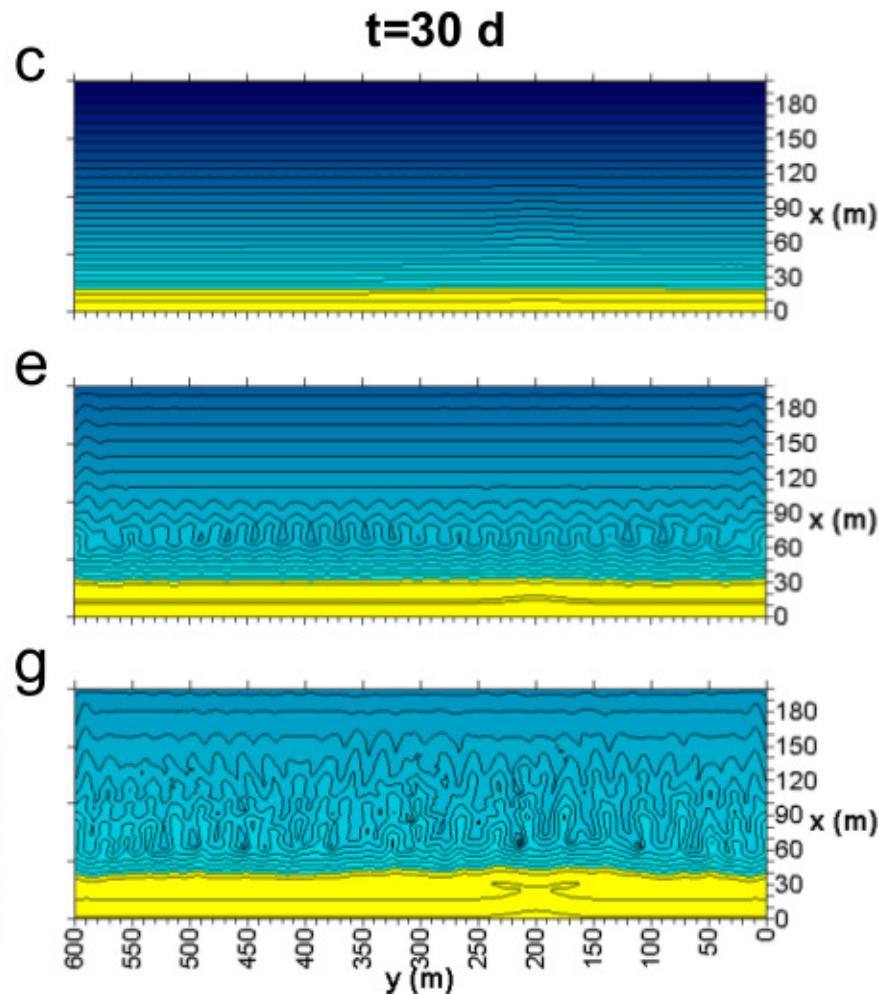
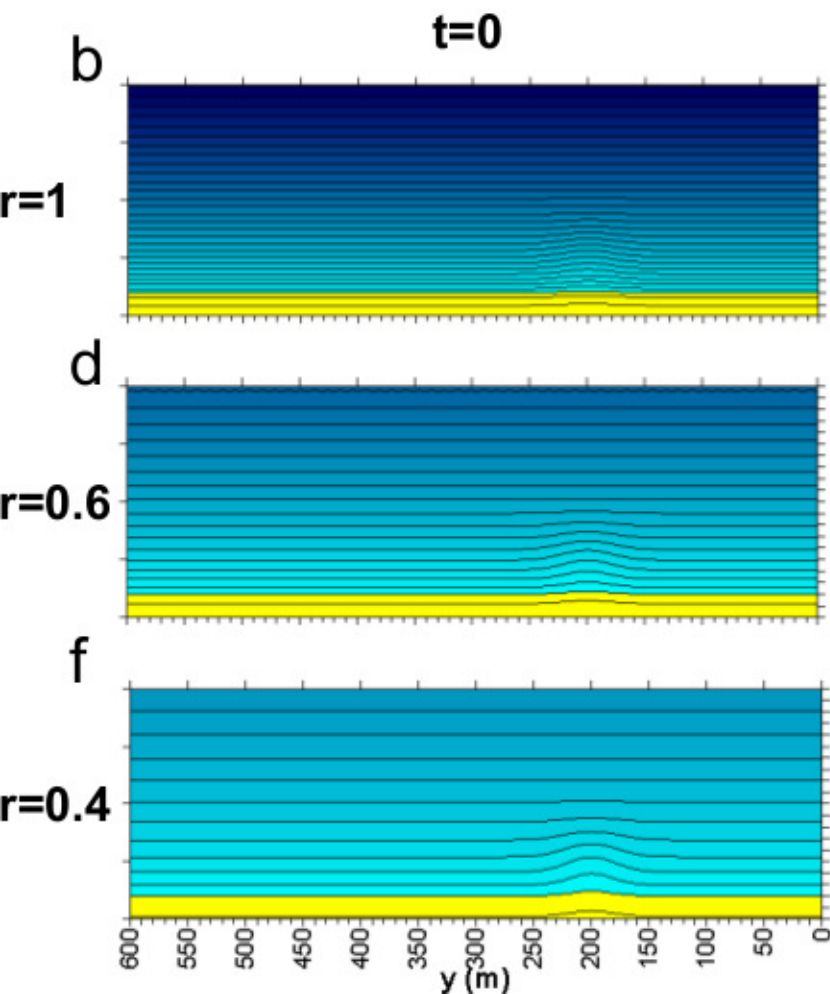
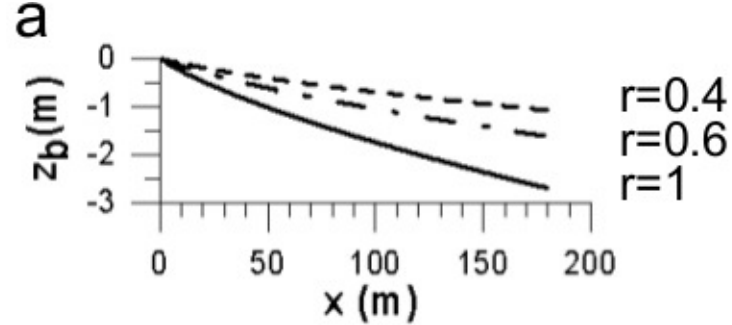


Figure 4.

